

Collinear spin density wave state in distorted square-lattice GdNiSn₄

Charles C. Tam,¹ Sarah Schwarz,¹ Xin Zhang,² Sudipta Chatterjee,² Scott B. Lee,² Rebecca Scatena,³ Leslie M. Schoop,² and Stephen D. Wilson¹

¹*Materials Department, University of California Santa Barbara, Santa Barbara 93106 USA*

²*Department of Chemistry, Princeton University, Princeton, New Jersey 08544, USA*

³*Diamond Light Source, Harwell Science and Innovation Campus, Didcot, Oxfordshire OX11 0DE, UK*

We characterize the magnetic ground state of the newly synthesized lanthanide intermetallic GdNiSn₄ via resonant elastic x-ray scattering measurements. This compound forms distorted square nets of Gd that initially order magnetically below 23 K followed by a lower temperature transition at 16 K. Our scattering data identify the ground state order as a single- \mathbf{q} incommensurate, collinear order that slides towards a commensurate wave vector above the 16 K transition. Magnetic symmetry analysis combined with azimuthal dependence resolves the ground state magnetic structure as a moment-modulated spin density wave state with Gd moments oriented parallel to the in-plane a -axis. We discuss connections between the observed magnetic order and electronic properties in this square-net compound.

I. INTRODUCTION

One strategy of engineering quantum materials that host unconventional magnetotransport phenomena is to embed a high symmetry network of local lanthanide moments, such as Gd, into crystal lattices that host high mobility (often topologically nontrivial) electronic band structures. The localized lanthanide moments hybridize and interact with the mobile conduction electrons and can often be described by a Hamiltonian with local Kondo and extended Ruderman-Kittel-Kasuya-Yosida (RKKY) interactions. A variety of noncoplanar spin textures can result and generate a finite scalar spin chirality, promoting a topological Hall response. The most widely studied manifestation of this occurs in non-centrosymmetric systems, where a global Dzyaloshinskii-Moriya interaction (DMI) is allowed and skyrmion topological spin textures may form. Common examples are found in B20 alloys such as MnSi and FeGe [1, 2], though a much broader range of compounds are known to exhibit similar phenomenology [3].

For the broader class of centrosymmetric lattices, non-coplanar spin textures and skyrmion phases may also form via RKKY interactions, even in the absence of a global DMI [4–6]. To date, various types of centrosymmetric lattices have been shown to host topological spin textures, particularly among geometrically frustrated lattices such as triangular Gd₂PdSi₃ [7, 8] and kagome Gd₃Ru₄Al₁₂ [9] with multi- \mathbf{q} order. More recently, similar phenomenology was discovered in tetragonal lattices that are free from conventional geometric frustration, with examples including EuAl₄ [10–12], EuGa₂Al₂ [13], GdRu₂Si₂ [14–17], and GdRu₂Ge₂ [18, 19]. This opens a door for an even larger pool of non-hexagonal, centrosymmetric compounds and motivates the use of square-nets of lanthanides as a building block for engineering topological spin textures into high-mobility intermetallic compounds as a means of creating unconventional Hall responses.

In a recent report, Zhang *et al.* synthesized and char-

acterized a new intermetallic compound GdNiSn₄ [20]. This compound is monoclinic and forms bilayers of distorted square-planes of Gd. They are slightly distorted square nets, because although the angle between a and b is 90°, the nearest neighbor Gd-Gd bond distance is inequivalent, with Gd-Gd along a being 4.4365 Å and 4.4037 Å along b (see Figure 1a). The nature of the ground state magnetic order and its evolution under magnetic field remain unknown.

In this paper, we determine the ground state magnetic structure of GdNiSn₄ and its evolution upon warming through T_{SDW} . Due to strong nuclear absorption associated with Gd ions, resonant elastic x-ray scattering (REXS) techniques were utilized rather than traditional neutron diffraction. Single- \mathbf{q} , incommensurate magnetic order is observed with moments modulated both within the Gd square-net ab -plane as well as along the inter-layer direction. Magnetic symmetry analysis combined with azimuthal dependence restricts the magnetic structure to a collinear spin density wave with moments parallel to the a -axis. The coupling of this magnetic structure to the electronic properties of GdNiSn₄ is discussed.

II. METHODS

GdNiSn₄ single crystals were grown via a Sn-based self-flux technique. More details on synthesis and characterization is given in Ref. 20. GdNiSn₄ crystallizes in the $C/2m$ space group, with two distinct Gd atoms on the $4i$ Wyckoff site. Here we label the c -axis as the long axis, and the ab -plane is the basal plane in which the Gd square nets reside.

Resistivity and specific heat data were collected using a Quantum Design Physical Property Measurement System (Dynacool PPMS). Resistivity measurements were performed a four-probe method with contacts created with silver paste, and data were collected using the electrical transport option of the PPMS. Specific heat measurements were performed using the quasi-adiabatic re-

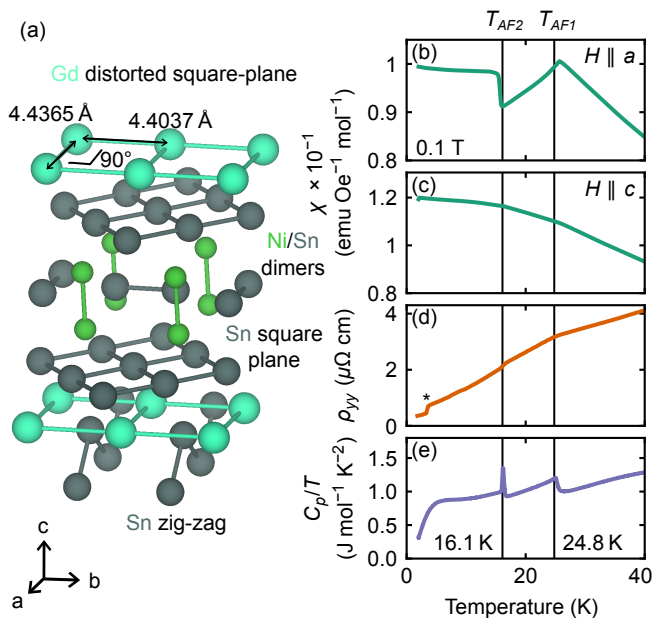


FIG. 1. **Physical properties of distorted square-lattice GdNiSn₄.** (a) Crystal lattice of GdNiSn₄ where differing structural motifs are labeled. The structure has been simplified for clarity; more detailed structural information is given in Ref. 20. Temperature dependent magnetic susceptibility with the applied field of $\mu_0 H = 0.1$ T is shown applied (b) parallel to the a -axis, (c) and parallel to the c -axis. (d) Zero field ρ_{yy} . Note the transition at ≈ 4 K (denoted by *), is a superconducting transition of residual Sn flux. (e) Specific heat capacity divided by temperature C_p/T collected at zero field.

laxation method and the crystal mounted within the heat capacity option of the PPMS. Orientation-dependent magnetization data were collected using a Quantum Design Magnetic Property Measurement System (MPMS3).

Resonant elastic x-ray scattering (REXS) measurements were performed at beamline I16, Diamond light source [21]. Samples were measured as as-grown and mounted in a reflection geometry, using a beam size of $\sim 180\mu\text{m} \times 25\mu\text{m}$ (width \times height). Specifically, samples were mounted such that the (001) was the specular direction, and (100) was the azimuthal reference. Samples were cooled with an ARS closed-cycle cryostat with a beryllium dome. Momentum transfer is labeled in reciprocal lattice units (r.l.u.) of the monoclinic unit cell of GdNiSn₄, where $\mathbf{Q} = H\mathbf{a}^* + K\mathbf{b}^* + L\mathbf{c}^*$, $a = 8.7409$ Å, $b = 8.8238$ Å, $c = 14.3341$ Å, and $\alpha = \gamma = 90^\circ$, $\beta = 98.77^\circ$. In a vertical scattering geometry, incident light from the undulator is horizontally polarized, and is therefore σ polarized with respect to the scattering plane. Linear polarization analysis was done using a graphite (006) crystal oriented close 44.4° , and the incident polarization was controlled using light transmitted through a $400\mu\text{m}$ diamond (001) plate oriented close to the (111) reflection in asymmetric Laue mode.

III. EXPERIMENTAL RESULTS

Measurements of the temperature dependent DC magnetic susceptibility of GdNiSn₄ are plotted in Figure 1(b,c). Consistent with measurements reported in [20], the data indicate antiferromagnetic order appears initially at $T_{AF1} \approx 25$ K with a second transition near $T_{AF2} \approx 16$ K. Orientation dependent measurements suggest an enhanced susceptibility within the ab -plane, and the two transitions are consistent with anomalies within the resistivity ρ_{yy} which is plotted in Figure 1d., and zero-field specific heat, which is plotted in Figure 1e.

In order to characterize the magnetic structure responsible for the anomalies in $C_p(T)$, resonant x-ray diffraction measurements were performed. The incident x-ray energy was tuned to the Gd- L_2 absorption peak near 7.933 keV, enhancing resonant scattering coming from the Gd atoms. After a thorough search through reciprocal space, an incommensurate peak was observed at $\mathbf{Q} = (0.56, 1, 10.22)$ and equivalent positions, demonstrating an incommensurate magnetic $\mathbf{q} = (0.06, 0, 0.22)$. In Figure 1c, a fixed- \mathbf{Q} energy scan on a magnetic Bragg reflection renders a distinct resonant profile, peaking slightly below Gd- L_2 edge (≈ 2 eV). Magnetic scattering is expected to rotate linearly polarized light by 90° , and in Figure 2c, polarization analysis of the scattered beam shows this to be the case. In a broader search of symmetry equivalent positions in different Brillouin zones, these peaks are only present at odd H (Figure 2d) and odd K (Figure 2e) zone centers while they exist for both even and odd L (Figure 1f).

The temperature dependence of the magnetic peak was measured and is plotted in Figure 3a. At 7.5 K, it becomes clear the magnetic peak is composed of a primary peak at $Q_1 = (0.56, 1, 10.22)$ with a secondary peak visible as a shoulder at $Q_2 = (0.56, 1, 10.18)$. Upon warming, scattering at Q_1 is suppressed with an order parameter-like behavior and is no longer detectable above $T_{AF2} = 13$ K. Meanwhile, upon warming the scattering along Q_2 grows in intensity and is peaked near 13 K. Warming up further, Q_2 is then subsequently suppressed until it is no longer detected around $T_{AF1} = 23$ K. This behavior is consistent when measured across equivalent positions in different zones (see supplementary information [22]). We note there is an apparent ≈ 3 K offset in the x-ray-derived transition temperatures relative to the T_{AF1} and T_{AF2} transitions identified from magnetization, heat capacity, and resistivity data in Figure 1. This apparent shift downward in the onset temperatures of transitions observed via x-ray scattering likely arises from local beam heating of the sample by the x-ray source.

Now turning to the incommensurability δ of the peaks (i.e. δ_L , where $L = 10 + \delta_L$) as a function of temperature in Figure 3c, both peaks at Q_1 and Q_2 show continuous changes when warmed; however the rate of change of Q_2 with temperature slows considerably when order along Q_1 vanishes and peak trends to a commensurate value of $\delta = 1/4$ as T_{AF2} is approached. Extrapolating linearly

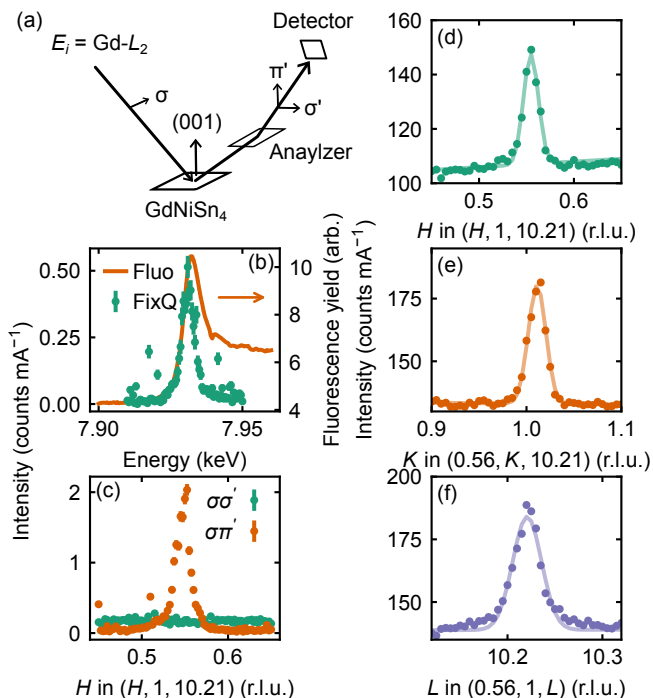


FIG. 2. **Incommensurate magnetic order in GdNiSn_4 .** (a) Scattering geometry and linear polarization analysis schematic. (b) Energy dependence of the $(0.56, 1, 10.22)$ peak, and fluorescence on the secondary axis. (c) H dependence of magnetic peak with $\sigma\sigma'$ and $\sigma\pi'$ incoming and outgoing polarization. (d)-(f) High symmetry cuts of the magnetic peak along H , K and L . All measurement were taken at 7.5 K.

to $T = 0$ K, Q_1 projects to a ground state incommensurability of $\delta \approx 0.18$, while the coexisting Q_2 harmonic becomes strongly suppressed. The in-plane wave vector remains fixed upon cooling through both phases at $\delta_H = 0.06$

REXS measurements further allow for an unambiguous measurement of the moment direction in the ordered state. This is accomplished by measuring the azimuthal dependence of the magnetic peak with different incident light polarization. At each azimuth value in the scan, a rocking curve is performed and the intensity integrated for the magnetic peak. The azimuthal value where the intensity is maximized is, to first order, the moment direction. A schematic of this is drawn in Figure 4a. An azimuthal measurement following this protocol was performed at 7.5 K to probe the moment orientation at $Q_1 = (0.56, 1, 10.22)$, and another at 20 K to ensure Q_1 was fully suppressed to probe the moment orientation at $Q_2 = (0.56, 1, 10.24)$.

The azimuthal dependence was first measured with circularly polarized light, with circular left (CL) and circular right (CR), polarizations. This is plotted in Figure 4b,d for measurements taken at 7.5 K and 20 K respectively. The absence of contrast between CL and CR is consistent with a collinear magnetic structure. With

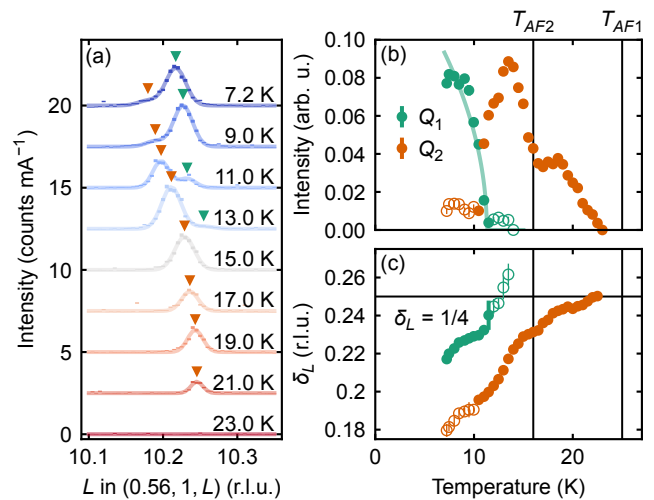


FIG. 3. **Temperature dependence of magnetic order of GdNiSn_4 .** L scans taken at different temperatures across the $(0.56, 1, 10.22)$ peak. The background has been subtracted and higher temperature scans have been offset for clarity. Solid lines are fits. Peak centers are marked. (b) Temperature dependence of the two fitted peak intensities. The solid green line as an order parameter fit to the Q_1 intensity, and the solid orange line is a Gaussian fit to the Q_2 intensity. (c) Temperature dependence of the two fitted peak centers. Hollow markers in (b) and (c) are the fitted values of the peak when intensity is too low compared to the other peak to be reliable.

linearly polarized σ and π light, there is a total suppression of intensity in the σ polarized light at around -90° . Since the azimuthal reference is along (100) , this means that the maximum in the σ polarized channel is near $\phi = 0^\circ$, and therefore that the moments are in the (a, c) plane. Given that the structure is collinear and the ordering wave vector is incommensurate, magnetic symmetry analysis dictates that the structure must be a moment modulated spin density wave (SDW) [22].

The cant direction of the SDW can be determined by fitting the azimuthal dependence to simulated x-ray scattering intensities. Using expressions from Hill and McMorrow [23] and taking into account absorption due to resonance, the azimuthal dependence of the data was fit to a model where moments are constrained to the (a, c) plane (where ϕ is the cant angle from the c axis). The result is plotted in Figure 4c where least squares fitting of this model to the data determines $\phi_1 = 99.9^\circ \pm 1.5^\circ$ at 7.5 K, and $\phi_2 = 103.5^\circ \pm 2.1^\circ$ at 20 K. This is within error of the monoclinic angle $\beta = 98.77^\circ$. Within error of the technique, the moment is parallel to a , and the lack of moment projected along c is consistent with the almost featureless $\chi(T)$ when field is applied along the c axis (Figure 1d). A representative picture of the resulting collinear magnetic structure in the mB_2 irrep is depicted in Figure 4d. We note that with our current REXS data, we are unable to determine the magnitude of the ordered moment that is modulated.

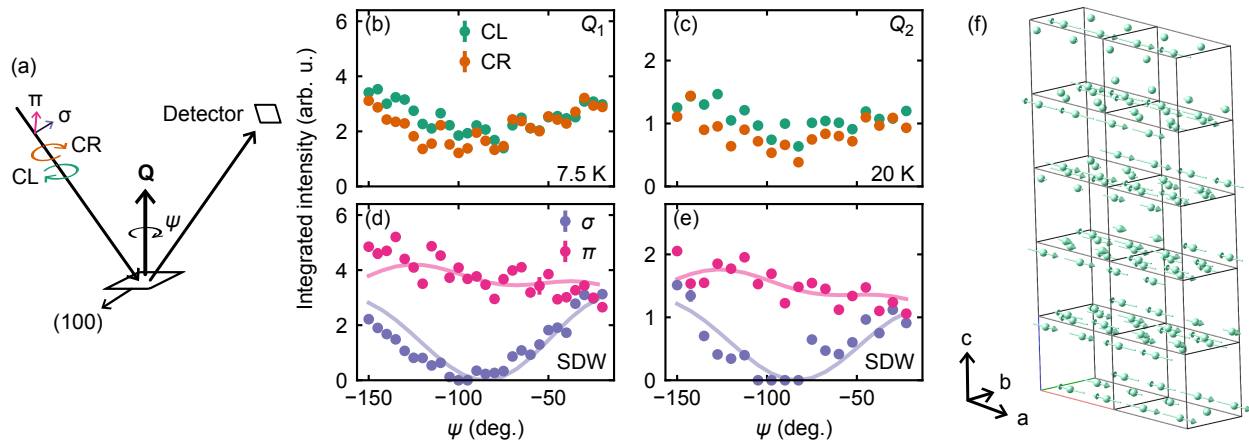


FIG. 4. **Determination of zero-field magnetic structure of GdNiSn₄.** (a) Scattering geometry schematic for azimuthal dependent scans with varying incident polarization and without polarization analysis. (b), (c) Integrated intensities of rocking curves on $Q_1 = (0.56, 1, 10.22)$ at 7.5 K and $Q_2 = (0.56, 1, 10.24)$ at 20 K, with circularly polarized incident light. (d), (e) Integrated intensities of rocking curves on Q_1 at 7.5 K and Q_2 at 20 K with linearly polarized light. Solid lines are fits to the proposed magnetic structure, with a best fit value of the cant angle $\phi_1 = 99.9^\circ \pm 1.5^\circ$ at 7.5 K, and $\phi_2 = 103.5^\circ \pm 2.1^\circ$ at 20 K. ϕ is the angle of the moments from the c axis. (f) Visualization of moment-modulated spin density wave structure, where $m \parallel a$. The c axis has been shrunk for clarity.

IV. DISCUSSION AND CONCLUSIONS

Sliding of magnetic ordering wave vectors often occurs in spin density wave systems and is reported in other Gd intermetallics [24]. A common tendency is for the wave vector to transition or slide toward a commensurate position as a means of minimizing entropy upon cooling. However, this is distinct from the case of GdNiSn₄ where the interplanar modulation moves away from commensuration upon cooling. This is likely due to the presence of an intermediate, first-order transition at $T_{AF2} \approx 13$ K.

There is an extended regime of coexistence between the T_{AF1} and T_{AF2} phases, indicating a first-order phase boundary and consistent with the sharp $C_P(T)$ anomaly shown in Figure 1 (e). This precludes the two Q s from corresponding to a single phase multi- Q structure (there are no peaks at $Q_1 + Q_2$), and instead indicates phase separation as the sample is cooled across T_{AF1} . The tradeoff in intensities between the two phases is consistent with a metastable regime where the modulation associated with T_{AF2} persists and a different harmonic appears closer to the commensurate point before the T_{AF2} order vanishes. We can also preclude that these two different Q s are associated with different crystallographic grains/twins. The twinning of the crystal we measured was captured with a twin law model, which gave a twinning ratio of 57.1/42.9 [22]. Although this is fairly even, and Q_1 and Q_2 have fairly consistent peak intensities, their temperature dependence's are distinct. Additionally, the small beam size allowed us to raster on the sample to a spot where no twinning was observed in the structural Bragg peaks in the areas probed by the x-ray beam. Additional details on the twinning model can be seen in the supple-

mentary information [22] and Ref. 20.

The two T_{AF1} and T_{AF2} states only differ in their modulation along the interplane direction and scattering from both states is consistent with a collinear spin density wave phase. Interplane coupling is likely much weaker given the lattice structure making the wavelength of the SDW more susceptible to either entropic effects or subtle changes in the electronic structure along this direction. Excluding GdRu₂Si₂ and GdRu₂Ge₂, a number of previously studied tetragonal Gd-based intermetallics are known to host antiferromagnetic ground states where the moments align in a basal plane, such as Gd₂IrIn₈ [25] or Gd₂CoGa₈ GdRhIn₅ [26] with examples of out-of-plane moment alignment in the layered compound GdMn₂Ge₂ [27]. A similar spin density wave state was found in GdNi₂B₂C [28] with an initial modulation that evolves upon cooling that is eventually interrupted by a spin-reorientation transition. A change in the moment direction of GdNiSn₄ is not resolved in our current data below T_{AF1} , though detecting a small, partial projection away from the a -axis may be beneath the resolution of our measurements.

A similar square lattice lanthanide compound EuAl₄ displays a cascade of magnetic phases in temperature and field [11], which include both non-collinear and SDW orders at zero field [29] in addition to a charge density wave (CDW) state [30]. While the isostructural system EuGa₄ is a simple antiferromagnet with no CDW phase [31], the lattice may be alloyed between the two extremes with Al substitution for Ga [32]. Along this alloy line, EuGa₂Al₂ shows a CDW with a SDW that condenses into a spin cycloid at low temperature [13, 33], and EuGa_{2.4}Al_{1.6} has a ground state SDW with coexisting helices at low temperatures, but without a CDW [34]. As a result, it is hy-

pothesized that a CDW distortion is required to stabilize the skyrmion phase in this system, and, indeed, a rectangular skyrmion lattice appears only in the orthorhombic phase of EuAl_4 [35, 36]. This highlights the role of lattice symmetry in the formation of magnetic phases. However, the corresponding tetragonal-to-orthorhombic distortion in EuAl_4 is much more subtle than the monoclinic distortion endemic to the lattice of GdNiSn_4 . This suggests that the two-fold in-plane rotational symmetry breaking is too strong in the case of GdNiSn_4 and serves to pin a single in-plane propagation wave vector.

In summary, we have investigated the zero-field magnetic structure of the newly reported square-net compound GdNiSn_4 [20]. REXS data reveal a collinear spin density wave state that is modulated both along the short in-plane and long interplane directions and whose mo-

ments are predominantly aligned along the in-plane propagation wave vector. The wave length of this longitudinal SDW slides upon cooling until an intermediate, first-order magnetic transition is reached and the out-of-plane period of modulation is shortened. Both magnetic transitions couple to electron transport in this compound and are likely driven via Fermi surface nesting effects. Our work provides an important zero-field picture of magnetic symmetry breaking in this compound essential for future work modeling field-dependent effects.

V. ACKNOWLEDGMENTS

This work was supported via AFOSR award FA9550-23-1-0635. We acknowledge beamtime at Diamond light source under proposal ID MM39446.

-
- [1] S. Mühlbauer, B. Binz, F. Jonietz, C. Pfleiderer, A. Rosch, A. Neubauer, R. Georgii, and P. Böni, Skyrmion lattice in a chiral magnet, *Science* **323**, 915 (2009).
- [2] X. Z. Yu, Y. Onose, N. Kanazawa, J. H. Park, J. H. Han, Y. Matsui, N. Nagaosa, and Y. Tokura, Real-space observation of a two-dimensional skyrmion crystal, *Nature* **465**, 901 (2010).
- [3] Y. Tokura and N. Kanazawa, Magnetic skyrmion materials, *Chemical Reviews* **121**, 2857 (2020).
- [4] R. Ozawa, S. Hayami, and Y. Motome, Zero-field skyrmions with a high topological number in itinerant magnets, *Physical Review Letters* **118**, 147205 (2017).
- [5] S. Hayami, R. Ozawa, and Y. Motome, Effective bilinear-biquadratic model for noncoplanar ordering in itinerant magnets, *Physical Review B* **95**, 224424 (2017).
- [6] Z. Wang, Y. Su, S.-Z. Lin, and C. D. Batista, Skyrmion crystal from RKKY interaction mediated by 2D electron gas, *Physical Review Letters* **124**, 207201 (2020).
- [7] T. Kurumaji, T. Nakajima, M. Hirschberger, A. Kikkawa, Y. Yamasaki, H. Sagayama, H. Nakao, Y. Taguchi, T.-h. Arima, and Y. Tokura, Skyrmion lattice with a giant topological Hall effect in a frustrated triangular-lattice magnet, *Science* **365**, 914 (2019).
- [8] M. Hirschberger, L. Spitz, T. Nomoto, T. Kurumaji, S. Gao, J. Masell, T. Nakajima, A. Kikkawa, Y. Yamasaki, H. Sagayama, H. Nakao, Y. Taguchi, R. Arita, T.-h. Arima, and Y. Tokura, Topological Nernst effect of the two-dimensional skyrmion lattice, *Physical Review Letters* **125**, 076602 (2020).
- [9] M. Hirschberger, T. Nakajima, S. Gao, L. Peng, A. Kikkawa, T. Kurumaji, M. Kriener, Y. Yamasaki, H. Sagayama, H. Nakao, K. Ohishi, K. Kakurai, Y. Taguchi, X. Yu, T.-h. Arima, and Y. Tokura, Skyrmion phase and competing magnetic orders on a breathing kagome lattice, *Nature Communications* **10**, 10.1038/s41467-019-13675-4 (2019).
- [10] A. Nakamura, T. Uejo, F. Honda, T. Takeuchi, H. Harima, E. Yamamoto, Y. Haga, K. Matsubayashi, Y. Uwatoko, M. Hedo, T. Nakama, and Y. Ōnuki, Transport and magnetic properties of EuAl_4 and EuGa_4 , *Journal of the Physical Society of Japan* **84**, 124711 (2015).
- [11] K. Kaneko, T. Kawasaki, A. Nakamura, K. Munakata, A. Nakao, T. Hanashima, R. Kiyonagi, T. Ohhara, M. Hedo, T. Nakama, and Y. Ōnuki, Charge-density-wave order and multiple magnetic transitions in divalent europium compound EuAl_4 , *Journal of the Physical Society of Japan* **90**, 064704 (2021).
- [12] R. Takagi, N. Matsuyama, V. Ukleev, L. Yu, J. S. White, S. Francoual, J. R. L. Mardegan, S. Hayami, H. Saito, K. Kaneko, K. Ohishi, Y. Ōnuki, T.-h. Arima, Y. Tokura, T. Nakajima, and S. Seki, Square and rhombic lattices of magnetic skyrmions in a centrosymmetric binary compound, *Nature Communications* **13**, 10.1038/s41467-022-29131-9 (2022).
- [13] J. M. Moya, S. Lei, E. M. Clements, C. S. Kengle, S. Sun, K. Allen, Q. Li, Y. Y. Peng, A. A. Husain, M. Mitrano, M. J. Krogstad, R. Osborn, A. B. Puthirath, S. Chi, L. Debeer-Schmitt, J. Gaudet, P. Abbamonte, J. W. Lynn, and E. Morosan, Incommensurate magnetic orders and topological Hall effect in the square-net centrosymmetric EuGa_2Al_2 system, *Physical Review Materials* **6**, 074201 (2022).
- [14] A. Garnier, D. Gignoux, N. Iwata, D. Schmitt, T. Shigeoka, and F. Zhang, Anisotropic metamagnetism in GdRu_2Si_2 , *Journal of Magnetism and Magnetic Materials* **140–144**, 899 (1995).
- [15] Y. Yasui, C. J. Butler, N. D. Khanh, S. Hayami, T. Nomoto, T. Hanaguri, Y. Motome, R. Arita, T.-h. Arima, Y. Tokura, and S. Seki, Imaging the coupling between itinerant electrons and localised moments in the centrosymmetric skyrmion magnet GdRu_2Si_2 , *Nature Communications* **11**, 10.1038/s41467-020-19751-4 (2020).
- [16] N. D. Khanh, T. Nakajima, X. Yu, S. Gao, K. Shibata, M. Hirschberger, Y. Yamasaki, H. Sagayama, H. Nakao, L. Peng, K. Nakajima, R. Takagi, T.-h. Arima, Y. Tokura, and S. Seki, Nanometric square skyrmion lattice in a centrosymmetric tetragonal magnet, *Nature Nanotechnology* **15**, 444 (2020).
- [17] N. D. Khanh, T. Nakajima, S. Hayami, S. Gao, Y. Yamasaki, H. Sagayama, H. Nakao, R. Takagi, Y. Mo-

- tome, Y. Tokura, T. Arima, and S. Seki, Zoology of multiple- Q spin textures in a centrosymmetric tetragonal magnet with itinerant electrons, *Advanced Science* **9**, 10.1002/advs.202105452 (2022).
- [18] A. Garnier, D. Gignoux, D. Schmitt, and T. Shigeoka, Giant magnetic anisotropy in tetragonal GdRu_2Ge_2 and GdRu_2Si_2 , *Physica B: Condensed Matter* **222**, 80 (1996).
- [19] H. Yoshimochi, R. Takagi, J. Ju, N. D. Khanh, H. Saito, H. Sagayama, H. Nakao, S. Itoh, Y. Tokura, T. Arima, S. Hayami, T. Nakajima, and S. Seki, Multistep topological transitions among meron and skyrmion crystals in a centrosymmetric magnet, *Nature Physics* **20**, 1001 (2024).
- [20] X. Zhang, S. B. Lee, S. Chatterjee, H. Pi, Y. Yang, F. Katmer, E. G. Ward, D. E. Widdowson, C. C. Tam, S. Schwarz, C. J. Pollak, J. M. Moya, G. Skorupskii, V. A. Kurlin, S. D. Wilson, B. A. Bernevig, and L. M. Schoop, Identification of an unreported structure type in GdNiSn_4 and its implications for materials prediction (2026), [arXiv:2603.05613 \[cond-mat.mtrl-sci\]](https://arxiv.org/abs/2603.05613).
- [21] S. P. Collins, A. Bombardi, A. R. Marshall, J. H. Williams, G. Barlow, A. G. Day, M. R. Pearson, R. J. Woolliscroft, R. D. Walton, G. Beutier, G. Nisbet, R. Garrett, I. Gentle, K. Nugent, and S. Wilkins, Diamond beamline I16 (materials & magnetism), in *AIP Conference Proceedings* (AIP, 2010) pp. 303–306.
- [22] [Supplemental information](#).
- [23] J. P. Hill and D. F. McMorrow, X-ray resonant exchange scattering: Polarization dependence and correlation function, *Acta Crystallographica Section A Foundations of Crystallography* **52**, 236 (1996).
- [24] Z. Porter, G. Pokharel, J.-W. Kim, P. J. Ryan, and S. D. Wilson, Incommensurate magnetic order in the Z_2 kagome metal GdV_6Sn_6 , *Physical Review B* **108**, 035134 (2023).
- [25] E. Granado, P. G. Pagliuso, C. Giles, R. Lora-Serrano, F. Yokaichiya, and J. L. Sarrao, Magnetic structure and fluctuations of Gd_2IrIn_8 : A resonant x-ray diffraction study, *Physical Review B* **69**, 144411 (2004).
- [26] E. Granado, B. Uchoa, A. Malachias, R. Lora-Serrano, P. G. Pagliuso, and H. Westfahl, Magnetic structure and critical behavior of GdRhIn_5 : Resonant x-ray diffraction and renormalization group analysis, *Physical Review B* **74**, 214428 (2006).
- [27] S. A. Granovsky, A. Kreyssig, M. Doerr, C. Ritter, E. Dudzik, R. Feyerherm, P. C. Canfield, and M. Loewenhaupt, The magnetic order of GdMn_2Ge_2 studied by neutron diffraction and x-ray resonant magnetic scattering, *Journal of Physics: Condensed Matter* **22**, 226005 (2010).
- [28] C. Detlefs, A. I. Goldman, C. Stassis, P. C. Canfield, B. K. Cho, J. P. Hill, and D. Gibbs, Magnetic structure of $\text{GdNi}_2\text{B}_2\text{C}$ by resonant and nonresonant x-ray scattering, *Physical Review B* **53**, 6355 (1996).
- [29] A. M. Vibhakar, D. D. Khalyavin, F. Orlandi, J. M. Moya, S. Lei, E. Morosan, and A. Bombardi, Spontaneous reversal of spin chirality and competing phases in the topological magnet EuAl_4 , *Communications Physics* **7**, 10.1038/s42005-024-01802-7 (2024).
- [30] S. Ramakrishnan, S. R. Kotla, T. Rekiş, J.-K. Bao, C. Eisele, L. Noohinejad, M. Tolkiehn, C. Paulmann, B. Singh, R. Verma, B. Bag, R. Kulkarni, A. Thamizhavel, B. Singh, S. Ramakrishnan, and S. van Smaalen, Orthorhombic charge density wave on the tetragonal lattice of EuAl_4 , *IUCrJ* **9**, 378 (2022).
- [31] T. Kawasaki, K. Kaneko, A. Nakamura, N. Aso, M. Hedo, T. Nakama, T. Ohhara, R. Kiyonagi, K. Oikawa, I. Tamura, A. Nakao, K. Munakata, T. Hanashima, and Y. Onuki, Magnetic structure of divalent europium compound EuGa_4 studied by single-crystal time-of-flight neutron diffraction, *Journal of the Physical Society of Japan* **85**, 114711 (2016).
- [32] M. Stavinoha, J. A. Cooley, S. G. Minasian, T. M. McQueen, S. M. Kauzlarich, C.-L. Huang, and E. Morosan, Charge density wave behavior and order-disorder in the antiferromagnetic metallic series $\text{Eu}(\text{Ga}_{1-x}\text{Al}_x)_4$, *Physical Review B* **97**, 195146 (2018).
- [33] A. M. Vibhakar, D. D. Khalyavin, J. M. Moya, P. Manuel, F. Orlandi, S. Lei, E. Morosan, and A. Bombardi, Competing charge and magnetic order in the candidate centrosymmetric skyrmion host EuGa_2Al_2 , *Physical Review B* **108**, 1100404 (2023).
- [34] M. T. Littlehales, S. H. Moody, P. J. Bereciartua, D. A. Mayoh, Z. B. Parkin, T. J. Blundell, E. Unsworth, S. Francoual, G. Balakrishnan, D. A. Venero, and P. D. Hatton, Spin density waves and ground state helices in $\text{EuGa}_{2.4}\text{Al}_{1.6}$, *Physical Review Research* **6**, 1032015 (2024).
- [35] S. Hayami, Orthorhombic distortion and rectangular skyrmion crystal in a centrosymmetric tetragonal host, *Journal of Physics: Materials* **6**, 014006 (2022).
- [36] M. Gen, R. Takagi, Y. Watanabe, S. Kitou, H. Sagayama, N. Matsuyama, Y. Kohama, A. Ikeda, Y. Onuki, T. Kurumaji, T.-h. Arima, and S. Seki, Rhombic skyrmion lattice coupled with orthorhombic structural distortion in EuAl_4 , *Physical Review B* **107**, 1020410 (2023).